



Spontaneous bending of piezoelectric nanoribbons: Mechanics, polarization, and space charge coupling

C. Majidi^{a,*}, Z. Chen^b, D.J. Srolovitz^c, M. Haataja^d

^a Princeton University, Princeton Institute for the Science and Technology of Materials (PRISM), Princeton, NJ 08544, USA

^b Princeton University, Department of Mechanical and Aerospace Engineering, Princeton Institute for the Science and Technology of Materials (PRISM), Princeton, NJ 08544, USA

^c Yeshiva University, Department of Physics, New York, NY 10033, USA

^d Princeton University, Department of Mechanical and Aerospace Engineering, Princeton Institute for the Science and Technology of Materials (PRISM), and the Program in Applied and Computational Mathematics, Princeton, NJ 08544, USA

ARTICLE INFO

Article history:

Received 26 July 2009

Received in revised form

10 October 2009

Accepted 29 November 2009

Keywords:

Nanomechanics

Piezoelectricity

Surface stress

Rod theory

Zinc-oxide

ABSTRACT

A theory is developed to explain the spontaneous bending of polar $\pm(0001)$ faceted wurtzite nanoribbons, including the widely studied case of zinc oxide (ZnO) nanoarcs and nanorings. A rigorous thermodynamic treatment shows that bending of these nanoribbons can be primarily attributed to the coupling between piezoelectric effects, electric polarization, and the motion of free charge originating from point defects and/or dopants. The present theory explains the following experimental observations: the magnitude and sign of curvature and how this curvature depends on film thickness and dopant concentration. Good agreement between theory and experiment is obtained with no adjustable parameters. We identify three regimes of bending behavior with distinct thickness dependence for bending radius that depend on free carrier density, film thickness, and elastic, piezoelectric and dielectric constants.

© 2009 Elsevier Ltd All rights reserved.

1. Introduction

Understanding the physical mechanisms that control the growth and structure of nanoscale structures is key in developing materials for novel applications. Of particular interest are single crystal nanoribbons or nanobelts of several compound semiconductors and ceramics, which have been observed to spontaneously bend into what have been referred to as nanoarcs and nanorings. These include hexagonal (wurtzite) ribbons that have polar $\pm(0001)$ faces and are composed of zinc oxide (ZnO) (Kong and Wang, 2003), gallium nitride (GaN) (Jian et al., 2007), and aluminum nitride (AlN) (Duan et al., 2005). Such observations have been made for nanoribbons where typical dimensions are thickness ~ 10 nm, width ~ 10 – 100 nm and length ~ 1 – 100 μ m. By *spontaneously bent*, we mean that the nanoribbons bend into circular arcs or rings to minimize the potential energy of the nanoribbon. Due to their unique combination of electrical, mechanical, and geometric properties, piezoelectric nanoribbons will likely play a significant role in emerging nanotechnologies, from nanoelectromechanical systems (NEMS) (Wang, 2004) to energy harvesting (Wang and Song, 2006). For an overview of piezoelectric nanoribbons and their applications, see Wang (2004).

In this paper, we carry out a comprehensive thermodynamic analysis to identify the relevant physical effects that govern this phenomena and distinguish between competing mechanisms that could (or have been argued to) produce

* Corresponding author. Tel.: +1 609 258 0494.

E-mail address: cmajidi@princeton.edu (C. Majidi).

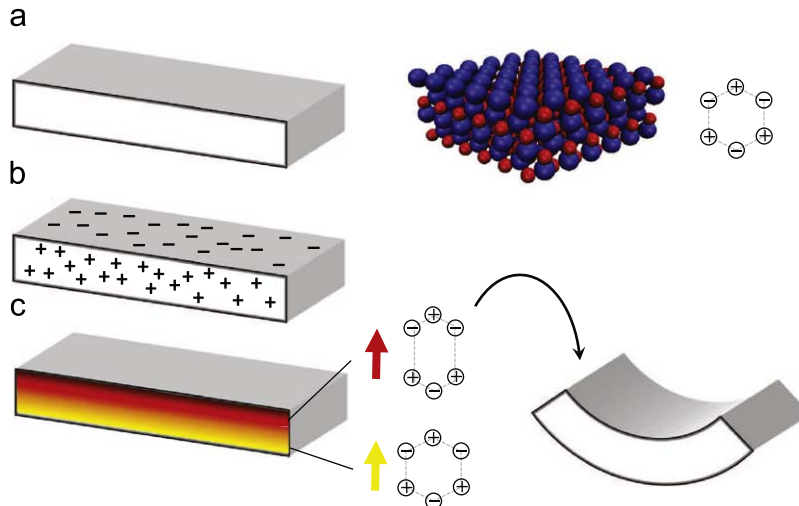


Fig. 1. Mechanism for spontaneous bending: (a) ZnO nanoribbon has a wurtzite crystal lattice with a non-centrosymmetric distribution of positively charged Zn ions and negatively charged O anions; (b) the free carriers move to neutralize surface polarity, leaving behind a depletion layer of oppositely charged lattice ions (Harris et al., 2000; Allen et al., 2007); (c) inside the depletion layer, the electric field varies linearly along the nanoribbon thickness and induces bending strain through piezoelectric coupling.

bending. Based on this analysis, we suggest that spontaneous bending is controlled by piezoelectric interactions and charge distributions in these materials. The theoretical predictions are consistent with the experimental observation that the radius of curvature is constant and on the order of $\sim 0.1\text{--}1\ \mu\text{m}$ (Hughes and Wang, 2004).

Previous studies have considered the contributions of elasticity, surface stress, electrostatics, and polarization-induced surface charge to the energetic stability of curved nanoribbons (Kong and Wang, 2004; Tu et al., 2006). Hughes and Wang (2004) reject the surface stress model to explain bending in ZnO ribbons, since it only allows bending towards a specific crystallographic direction, whereas bending is experimentally observed towards both the Zn-terminated (0001) or O-terminated (000 $\bar{1}$) surfaces. Also, as demonstrated in the current analysis, electrostatic effects generated by polarization-induced surface charge effectively increase the bending stiffness of the nanoribbon and do not lead to spontaneous bending. This is in contrast to the suggestions of Kong and Wang (2004), who assume that surface charge density remains fixed during bending. In the current analysis, we employ the more physical postulate that surface charge is fixed to the crystal lattice, such that total surface charge and not surface charge density is preserved during bending.

Here, we present a comprehensive theory that, in addition to elasticity, surface stress, electrostatics, and surface charge, also includes the energetic contributions of piezoelectricity and space charge.¹ While previous studies have ignored such effects, the current analysis clearly demonstrates that they are necessary for explaining the spontaneous bending observations. Interestingly, observations show that ZnO nanoribbons that are doped with impurities (such as indium) bend, while undoped ZnO ribbons do not (Kong et al., 2004; Wang, 2004).

The theory suggests that spontaneous bending is governed by piezoelectric interactions induced by local space charge. In the case of a charge neutral bulk, local space charge may be induced by the accumulation of charge carriers that leave behind lattice ions of opposite charge, resulting in a non-uniform charge distribution. Experimental measurements performed on ZnO nanowires indicate a charge carrier density as high as $\sim 10^{27}/\text{m}^3$ (Konenkamp et al., 2000). According to the theory, carrier densities at or within 1–2 orders of magnitude below this value can lead to radii of curvature of the same magnitude as those observed experimentally ($\sim 0.1\text{--}10\ \mu\text{m}$). This is the first theory that successfully reproduces a wide range of experimental observations: (1) the magnitude and sign of the experimentally measured radii of curvature, (2) how this curvature depends on nanoribbon thickness, and (3) the dependence of the sign and magnitude of the curvature on dopants.

In our theory, spontaneous bending arises through the following mechanism, which is illustrated in Fig. 1. First, the wurtzite structure of the nanoribbon (Fig. 1 a) induces an electric field with components perpendicular to the polar surfaces. This causes mobile charges to accumulate on one of the polar faces, depending on the sign of the charge carrier (Fig. 1 b). Uniform carrier depletion induces an internal electric field that varies linearly across the nanoribbon thickness (Fig. 1 c). Because of the piezoelectric coupling, this gradient in the electric field is accompanied by a gradient in the elastic strain that results in uniform nanoribbon bending (Fig. 1 c). The theory also identifies three different regimes of

¹ By local space charge, we mean net electric charge in a region (arising from, e.g., point defects or dopants) that is large compared to the distance between atoms, yet smaller than the dimensions of the ribbon.

deformation, for which the bending radius is either (I) independent of nanoribbon thickness, (II) linearly proportional to it, or (III) scales quadratically with it. While the crossover behavior between these regimes is controlled by the details of the mobile charge distribution, the asymptotic regime (III) is universal and governs the bending behavior of all piezoelectric and polar materials with sufficiently large thickness. In addition to planar bending, the theory provides a rigorous framework to examine non-planar nanoribbon geometries such as nanosprings and helices and to describe the effects of lattice defects.

The rest of the article is organized as follows. Following a derivation of the governing equations in Section 2, we present the kinematics for the planar bending of a nanoribbon (Section 3). Closed-form solutions for deformations are then obtained for the special cases of surface stress (Section 4), surface charge (Section 5), and space charge (Section 6). Finally, Section 7 contains a brief discussion, while details of some of the more involved calculations and derivations can be found in the Appendices.

2. Governing equations

In order to derive the governing equations for nanoribbon bending, we first consider a generalized piezoelectric body embedded in a fixed, global Cartesian frame $\{\mathbf{e}_1, \mathbf{e}_2, \mathbf{e}_3\}$. In the reference configuration \mathcal{B}_0 , material points occupy positions $\mathbf{X} \in \mathcal{B}_0$. From \mathcal{B}_0 , the points undergo elastic displacement $\mathbf{u} = \mathbf{u}(\mathbf{X})$ to a final position $\mathbf{x} = \boldsymbol{\chi}(\mathbf{X}) = \mathbf{X} + \mathbf{u}$ in the energetically favorable and mechanically stable configuration \mathcal{B} . Here, $\boldsymbol{\chi} : \mathcal{B}_0 \rightarrow \mathcal{B}$ represents the deformation mapping of material points to their spatial coordinates in \mathcal{B} and is assumed to be invertible. In addition to kinematic displacement, there is an electric potential $\Phi = \Phi(\mathbf{X})$ associated with material points.

The energy density of the nanoribbon is a function of the second-order strain tensor $\boldsymbol{\gamma}$ and electric intensity vector \mathbf{E} . For arbitrary displacements but small strain $\boldsymbol{\gamma}$ is approximated by the infinitesimal strain tensor:

$$\boldsymbol{\gamma} = \frac{1}{2}\{\nabla\mathbf{u} + \nabla\mathbf{u}^\top\}, \quad (1)$$

where $\nabla\mathbf{u} = \mathbf{F} - \mathbf{I}$ is the displacement gradient, $\mathbf{F} = \nabla\boldsymbol{\chi} = \boldsymbol{\chi} \otimes \nabla$ is the deformation gradient, and \mathbf{I} is the second-order identity tensor (Bertram, 2005). Here, ∇ is defined as the gradient operator with respect to the material coordinate system and \otimes is the dyadic product ($\mathbf{Q} = \mathbf{u} \otimes \mathbf{v}$ where $Q_{ij} = u_i v_j$). The operator ∇ is also used to compute the electric intensity in the material description:

$$\mathbf{E} = -\nabla\Phi. \quad (2)$$

Since $\boldsymbol{\gamma}$ and \mathbf{E} are treated as independent variables, the energy density corresponds to the enthalpy density (Pak, 1992; Jogai et al., 2004):

$$h = \frac{1}{2}\boldsymbol{\gamma} : \mathbf{C} : \boldsymbol{\gamma} - \mathbf{E} \cdot (\mathbf{g} : \boldsymbol{\gamma}) - \frac{1}{2}\boldsymbol{\varepsilon} \cdot (\boldsymbol{\varepsilon} \cdot \mathbf{E}) - \mathbf{P}_0 \cdot \mathbf{E}. \quad (3)$$

Here, \mathbf{C} is the fourth-order stiffness tensor, \mathbf{g} is the third-order piezoelectric coupling tensor, $\boldsymbol{\varepsilon}$ is the second-order electric permittivity tensor, \mathbf{P}_0 is the vector for spontaneous polarization and the double contraction ($:$) in the tensor $\mathbf{C} : \boldsymbol{\gamma}$ has components $C_{ijkl} \gamma_{kl}$ (and similarly for tensors of other ranks). These tensors have the following symmetry properties (Ding and Chen, 2001):

$$C_{ijkl} = C_{ijlk} = C_{jikl} = C_{klij}, \quad g_{ijk} = g_{ikj}, \quad \varepsilon_{ij} = \varepsilon_{ji}. \quad (4)$$

Lastly, the second-order stress tensor \mathbf{T} and electric displacement vector \mathbf{D} are related to $\boldsymbol{\gamma}$ and \mathbf{E} through the constitutive equations, which in view of (3) and (4), may be expressed as

$$\mathbf{T} = \frac{\partial h}{\partial \boldsymbol{\gamma}} = \mathbf{C} : \boldsymbol{\gamma} - \mathbf{E} \cdot \mathbf{g}, \quad (5)$$

$$\mathbf{D} = -\frac{\partial h}{\partial \mathbf{E}} = \mathbf{g} : \boldsymbol{\gamma} + \boldsymbol{\varepsilon} \cdot \mathbf{E} + \mathbf{P}_0. \quad (6)$$

It is important to note that the stress tensor is symmetric, i.e., $\mathbf{T} = \mathbf{T}^\top$. Also, as apparent in the expression for \mathbf{D} , the total polarization of the crystal is divided into a linear dielectric term, which is contained in $\boldsymbol{\varepsilon} \cdot \mathbf{E}$, and a constant \mathbf{P}_0 associated with spontaneous polarization. This representation of polarity is widely used in the literature for both piezoelectric and ferroelectric materials (Bernardini et al., 1997; Huber et al., 1999; Jogai et al., 2004).

In addition to the free variables $\boldsymbol{\gamma}$ and \mathbf{E} , the following fields in the body are prescribed: space charge density ρ , surface charge density σ (including surface charge associated with spontaneous polarization), and surface traction $\hat{\mathbf{t}}$. Here, the hat over a variable \hat{q} indicates that q takes on a prescribed value and is not a free variable. The total potential energy of the nanoribbon is (Ding and Chen, 2001)

$$\Pi = \int_{\mathcal{B}} \{h + \rho\Phi\} dV + \int_{\partial\mathcal{B}} \{\sigma\Phi - \hat{\mathbf{t}} \cdot \mathbf{u}\} dS. \quad (7)$$

Here, the inverse mapping $\mathbf{X} = \boldsymbol{\chi}^{-1}(\mathbf{x})$ is used to evaluate terms on \mathcal{B} that are otherwise defined in the material description. At equilibrium, Π must be stationary with respect to variations in \mathbf{u} and Φ . Consider variations of the form

$$\mathbf{u} \rightarrow \mathbf{u} + \delta \mathbf{u}, \quad \nabla \mathbf{u} \rightarrow \nabla \mathbf{u} + \nabla \delta \mathbf{u}, \quad \Phi \rightarrow \Phi + \delta \Phi \quad \text{and} \quad \nabla \Phi \rightarrow \nabla \Phi + \nabla \delta \Phi. \quad (8)$$

As shown in Appendix A, the corresponding variation in Π vanishes if and only if the balance equations

$$\nabla \cdot \mathbf{T} = \mathbf{0} \quad \text{in } \mathcal{B}, \quad \mathbf{T} \cdot \mathbf{n} = \hat{\mathbf{t}} \quad \text{on } \partial \mathcal{B} \quad (9)$$

and

$$\nabla \cdot \mathbf{D} = \rho \quad \text{in } \mathcal{B}, \quad \mathbf{D} \cdot \mathbf{n} = -\sigma \quad \text{on } \partial \mathcal{B} \quad (10)$$

are satisfied. Here, \mathbf{n} represents the unit normal to $\partial \mathcal{B}$. As expected, Eqs. (9) and (10) are the differential and boundary forms for the stress balance and Gauss's law, respectively. Nonetheless, to specialize these to the curved nanoribbon, below, it will be necessary to restrict the underlying kinematics. Finally, a finite surface stress $\hat{\mathbf{T}}$ can be incorporated to the theory by introducing a surface layer of finite thickness with a modified constitutive equation $\mathbf{T} = \mathbf{C} : \boldsymbol{\gamma} - \mathbf{E} \cdot \hat{\mathbf{T}}$.

3. Nanoribbon model

The nanoribbon is modeled as an extensible, planar, rod of length L , width w , and thickness H . The centerline is treated as a directed (Cosserat) curve whose orientation is defined by the body-fixed orthonormal directors $\{\mathbf{d}_1, \mathbf{d}_2, \mathbf{d}_3\}$. In the reference configuration \mathcal{B}_0 , these coincide with the Cartesian bases $\{\mathbf{e}_1, \mathbf{e}_2, \mathbf{e}_3\}$. Deformation is restricted to the $\mathbf{e}_1 - \mathbf{e}_3$ plane, and so the director \mathbf{d}_2 will always coincide with \mathbf{e}_2 . Furthermore, upon the deformation from \mathcal{B}_0 to \mathcal{B} , cross-sections are assumed to remain planar and perpendicular to the center line.

Material points are uniquely identified by a set of curvilinear coordinates $\{\xi, y, z\}$ and the gradient operator has the form $\nabla = \partial/\partial \xi \mathbf{d}_1 + \partial/\partial y \mathbf{d}_2 + \partial/\partial z \mathbf{d}_3$. As shown in Fig. 2, the nanoribbon is flat in its reference configuration \mathcal{B}_0 and forms a circular arc of uniform curvature in the final configuration \mathcal{B} . The centerline has an arclength $\xi \in [0, L]$, slope $\theta = \theta(\xi)$, and curvature $\kappa = d\theta/d\xi$. The director \mathbf{d}_1 is defined as tangent to the centerline:

$$\mathbf{d}_1 = \cos \theta \mathbf{e}_1 + \sin \theta \mathbf{e}_3. \quad (11)$$

Also, \mathbf{d}_3 is normal to the midplane of the nanoribbon and towards the direction of positive curvature:

$$\mathbf{d}_3 = \mathbf{d}_1 \times \mathbf{d}_2 = -\sin \theta \mathbf{e}_1 + \cos \theta \mathbf{e}_3. \quad (12)$$

For $\pm(0001)$ faceted crystals, \mathbf{d}_3 is directed along $[0001]$ or the c -axis.

In addition to a constant bending curvature κ , the nanoribbon is subject to a constant elongation strain γ_0 along \mathbf{d}_1 and a thickness contraction strain $\gamma_{33} = \gamma_{33}(z)$ along \mathbf{d}_3 . Thus, the strain tensor is restricted to the form

$$\boldsymbol{\gamma} = \gamma_{11} \mathbf{d}_1 \otimes \mathbf{d}_1 + \gamma_{33} \mathbf{d}_3 \otimes \mathbf{d}_3, \quad (13)$$

where $\gamma_{11} = \gamma_{11}(z) = \gamma_0 - \kappa z$ and $\gamma_{33} = \gamma_{33}(z)$. Also, the electric intensity becomes

$$\mathbf{E} = E_1 \mathbf{d}_1 + E_3 \mathbf{d}_3, \quad (14)$$

where $E_1 = \partial \Phi / \partial \xi$ and $E_3 = \partial \Phi / \partial z$. Finally, in the absence of shear strains and normal strain along \mathbf{d}_2 , the constitutive equations for a wurtzite crystal reduce to (Ding and Chen, 2001)

$$T_{11} = C_{11} \gamma_{11} + C_{13} \gamma_{33} - g_{31} E_3, \quad (15)$$

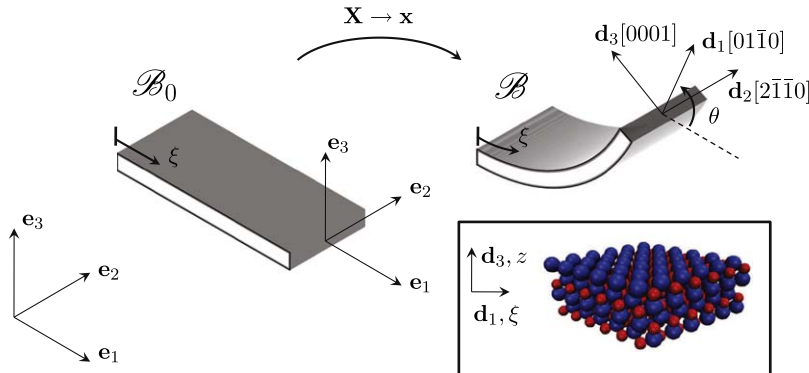


Fig. 2. The nanoribbon is treated as an elastic membrane with slope $\theta = \theta(\xi)$. \mathcal{B}_0 refers to the flat reference configuration with coordinate system \mathbf{X} and \mathcal{B} to the instantaneous curved body composed of points $\mathbf{x} = \mathbf{X} + \mathbf{u}$. The illustration in the inset is a schematic of the ZnO lattice structure viewed along $[2\bar{1}\bar{1}0]$, where the red and blue circles represent O^{2-} and Zn^{2+} ions, respectively. (For interpretation of the references to color in this figure legend, the reader is referred to the web version of this article.)

$$T_{33} = C_{13}\gamma_{11} + C_{33}\gamma_{33} - g_{33}E_3, \quad (16)$$

$$T_{13} = T_{31} = -g_{15}E_1, \quad (17)$$

$$D_1 = \varepsilon_{11}E_1, \quad (18)$$

$$D_3 = g_{31}\gamma_{11} + g_{33}\gamma_{33} + \varepsilon_{33}E_3 + P_0. \quad (19)$$

Here, Voigt notation has been used: $C_{ijkl} = C_{mn}$ and $g_{kij} = g_{km}$, where $m = \{i \text{ if } i=j, 5 \text{ otherwise}\}$ and $n = \{k \text{ if } k=l, 5 \text{ otherwise}\}$ and $i, j \in \{1, 3\}$. Also note that spontaneous polarization $\mathbf{P}_0 = P_0 \mathbf{d}_3$ only occurs in the \mathbf{d}_3 direction.

Subsequent calculations are based on the material constant for ZnO. For bulk ZnO, $C_{11} = 210$ GPa, $C_{13} = 105$ GPa, $C_{33} = 211$ GPa, $g_{31} = -0.61$ C/m², $g_{33} = 1.14$ C/m², $\varepsilon_{33} = 7.38 \times 10^{-11}$ F/m (Ding and Chen, 2001) and the spontaneous polarization $P_0 = 0.057$ C/m² (Bernardini et al., 1997).

4. Surface stress

We first analyze the role of surface stress on nanoribbon bending. Surface stress is defined as the variation of the surface free energy with respect to strain and is a two-dimensional, second order tensor. Physically, nonzero surface stresses arise because the atomic configurations and atomic bonding on the surface differs from those in the bulk crystal (Cahn and Hanneman, 1964). In non-centrosymmetric crystals, opposite crystal faces may have different surface stresses.

Surface stress along the length of the nanoribbon can be represented as an internal stress $\hat{\mathbf{T}} = \hat{T}_{11}(z) \mathbf{d}_1 \otimes \mathbf{d}_1$, where

$$\hat{T}_{11} = \lim_{\tau \rightarrow 0} \begin{cases} f_a/\tau, & z \in [a-\tau, a], \\ 0, & z \in (b+\tau, a-\tau), \\ f_b/\tau, & z \in [b, b+\tau], \end{cases} \quad (20)$$

$a = H/2$, $b = -H/2$, the constants f_a and f_b have dimensions of force per length, and τ is the surface thickness. Because $\hat{\mathbf{T}}$ is not smooth, it is necessary to rederive the governing equations related to variations in the displacement \mathbf{u} (Gauss's law, however, still remains valid). This is accomplished by obtaining an algebraic expression for the potential energy $\Pi = \Pi(\gamma_0, \kappa)$ and then solving the equilibrium conditions $\partial\Pi/\partial\gamma_0 = \partial\Pi/\partial\kappa = 0$ for γ_0 and κ . This yields (see Appendix B for derivation)

$$\gamma_0 = \frac{f_a + f_b}{\bar{C}H} \quad \text{and} \quad \kappa = \frac{6(f_b - f_a)}{\bar{C}H^2}, \quad (21)$$

where \bar{C} (B.3) is the effective elastic modulus and takes into account both elastic stiffness and piezoelectric coupling. Using bulk parameters for ZnO, \bar{C} is calculated to be 175 GPa.

The equations in (21) give the relationship between the nanoribbon stretch (γ_0) and bending curvature (κ) as a function of the surface stresses f_a and f_b , which act on the $z = a$ (Zn-terminating) and $z = b$ (O-terminating) surfaces, respectively. It is interesting to note that using a simple stress-strain argument, Cahn and Hanneman (1964) predict that the equilibrium curvature is $\kappa \approx 6(f_b - f_a)/YH^2$, where $Y = C_{11} - C_{13}^2/C_{33}$ is Young's modulus. This is close to the result obtained from the general energy analysis here, but with the effective elastic modulus \bar{C} replaced by Y . The difference occurs because Cahn and Hanneman (1964) do not include piezoelectric couplings in their derivation. Indeed, if the piezoelectric coupling coefficients (g_{ij}) vanish, then \bar{C} reduces to Y , which is equivalent to the bending modulus corrected for plane stress.

While surface stress values have not been measured (to our knowledge) for ZnO (0001), experience in a range of physical systems suggest that $|f_a|$ and $|f_b|$ should each be no larger than a few N/m (J/m²) (Cahn and Hanneman, 1964). For a ZnO nanoribbon of thickness $H = 10$ nm and $|f_b - f_a| \approx 1$ N/m, $R = 1/\kappa \approx 3$ μm which is an order of magnitude greater than the smallest values observed experimentally (~ 350 nm). Moreover, surface stresses only allow bending towards a specific crystallographic direction, i.e., the direction with the smaller value for f . In contrast, experimental observations reveal that ZnO nanoribbons can bend towards either the Zn-terminated (0001) or O-terminated (000 $\bar{1}$) surface (Hughes and Wang, 2004). Hence, we do not expect surface stresses to be the dominant source of ZnO nanoribbon bending. Of course, we cannot rule out the possibility that adsorbates or massive reconstructions of the two polar surfaces may affect the relative magnitudes of f_a and f_b , leading to bending towards either surface.

5. Surface charge

Another possible explanation for nanoribbon bending considered in the literature concerns surface charge induced by spontaneous polarization. As discussed in Wang (2004) and illustrated in the inset to Fig. 2, the wurtzite structure of ZnO may be described as a stack of alternating planes of O^{2-} and Zn^{2+} ions. Hence, the $z = a \equiv H/2$ and $z = b \equiv -H/2$ surfaces will contain a bound sheet charge of P_0 and $-P_0$, respectively.

Polarization induced surface charge can influence nanoribbon energetics in several ways. One approximation treats the nanoribbon as a capacitor in which the stored electrostatic energy depends on the radius of curvature. This model was introduced by Kong and Wang (2004) and is summarized below in Section 5.1. Lastly, surface charge and polarization can induce elastic strain through piezoelectric coupling. This is analyzed in Section 5.2 using the results of the energy analysis.

In all the aforementioned cases, the model calculations confirm the key result that neither surface charge nor spontaneous polarization are sufficient for nanoribbon bending. In fact, as with elastic strain, they actually introduce an energetic penalty to bending and effectively increase the bending stiffness.

5.1. Capacitor model

The divergence of the polarization at the {0001} faces of the nanoribbon implies that these surface are charged. Hence, the nanoribbon can be treated as a capacitor. Neglecting edge effects, the stored electrostatic energy is $\phi = Q^2/2C$, where $Q = \sigma wL$ is the total charge stored on either surface and C is the capacitance. For a flat nanoribbon, $C = \epsilon_{33}wL/H$, where ϵ_{33} is the electric permittivity. Assuming that the nanoribbon forms a circular ring of radius $|R| = L/2\pi$, the capacitance becomes $C = 2\pi\epsilon_{33}w/\ln(R_2/R_1)$, where $R_1 = |R| - H/2$ and $R_2 = |R| + H/2$ are the inner and outer radii, respectively. Here we adopt the convention that the inside of the ring corresponds to the Zn-terminated face when R is positive and to the O-terminating face when R is negative.

Noting that $Q = \sigma w(2\pi|R|)$, it follows that the electrostatic energy increases (relative to the planar nanoribbon) by an amount

$$\Delta\phi = \frac{Q^2}{4\pi\epsilon_{33}w} \left\{ \ln\left(\frac{1+\beta}{1-\beta}\right) - 2\beta \right\} \approx \frac{\pi w \sigma^2 H^3}{12\epsilon_{33}|R|}, \quad (22)$$

when the ribbon is bent into a ring, where $\beta = H/2|R|$. The total increase in potential energy upon bending the ribbon into a ring is obtained by combining the change in the elastic and electrostatic energies. This yields

$$\Delta\Pi = C^* \frac{\pi w H^3}{12|R|} \quad \text{where } C^* = Y + \frac{\sigma^2}{\epsilon_{33}}. \quad (23)$$

That is, the electrostatic effects induced by surface charge alone results in an effective increase in Young's modulus. Hence, *electrostatic effects as represented in the capacitor model always increase the bending stiffness and reduce the tendency for nanoribbon bending*. Moreover, the contribution to the overall potential energy will be negligible compared to that of elastic bending. Bending a ZnO nanoribbon of thickness $H = 10$ nm and width $w = 50$ nm into a ring of radius $R = 1$ μm increases the electrostatic energy by 6×10^{-19} J, which is four orders of magnitude less than the increase of 2×10^{-15} J in elastic strain energy.

In their derivation, Kong and Wang (2004) make the explicit assumption that surface charge density rather than surface charge remains fixed during bending. While this would lead to bending, in accordance with their conclusion, such an assumption has not yet been justified theoretically or confirmed experimentally. In fact, if the surface charge arises from the polarization inside the ribbon, the surface charge would be constant (as we assume) and in contradiction to the assumption of Kong and Wang (2004).

5.2. Piezoelectricity

Lastly, surface charge and spontaneous polarization can interact with elastic strain through the piezoelectric coupling. In order to evaluate the contributions of these effects alone, we ignore space charge, surface stress, and boundary tractions, i.e., $\rho = \dot{\mathbf{T}} = \dot{\mathbf{t}} = 0$. Also, since P_0 is already included in the constitutive equation for D_3 (19), we do not explicitly consider the spontaneous polarization as contributing to the surface charge. Rather, any charge on the surface that is present for any reason other than the spontaneous polarization is considered as surface charge σ_0 . Such charge may come from within the crystal (e.g., from dopants or point defects) or from external adsorbants (Noguera, 2000). The former will lead to space charge inside the bulk of the material, which is the subject of Section 6. In the present subsection, we assume that any surface charge σ_0 is associated with externally introduced surface adsorbents or from an electrolytic solution in which the nanoribbon is immersed. Surface polarity is completely canceled when $\sigma_0 = P_0$.

As the nanoribbon stretches and bends, the surface charge density σ changes such that the total charge on the surface remains fixed. In the Eulerian (deformed) description, $\sigma(a) = \sigma_0\{1 - \gamma_{11}(a)\}$, $\sigma(b) = -\sigma_0\{1 - \gamma_{11}(b)\}$, and $D_3 = -\sigma_0(1 - \gamma_{11})$, where $\gamma_{11} = -\kappa z$. The electric displacement must also satisfy the condition $D_3 = P_0 - \eta(\gamma_0 - \gamma_{11})$, which is derived from the constitutive equations when $\mathbf{T} = 0$.² The constant η is defined in Eq. (C.8) and is evaluated for prescribed piezoelectric coefficients. These two expressions for D_3 must simultaneously hold for all $z \in [-H/2, H/2]$ and imply

$$\gamma_0 = \frac{P_0 + \sigma_0}{\eta} \quad \text{and} \quad \kappa = 0. \quad (24)$$

² The condition $\mathbf{T} = 0$ is obtained by simultaneously solving the stress balance $\nabla \cdot \mathbf{T} = 0$, boundary condition $\mathbf{T} \cdot \mathbf{n} = 0$, constitutive law $\mathbf{T} = \mathbf{C} : \gamma - \mathbf{E} \cdot \mathbf{g}$, and compatibility condition $\nabla \times \mathbf{E} = 0$.

In other words, *while surface charge does lead to an overall stretching of the nanoribbon, it alone does not induce any bending curvature.* This result is consistent with the models presented in Sections 5.1. Using physical constants for ZnO ($\eta = 11.85 \text{ C/m}^2$ and $P_0 = 0.057 \text{ C/m}^2$), this implies that in the absence of surface charge ($\sigma_0 = 0$) $\gamma_0 = 0.005$ or a shortening of the nanoribbon by half of a percent. However, if the nanoribbon is placed in a charged environment that completely neutralizes the polarization ($\sigma_0 = -P_0$), then the stretching strain γ_0 is identically zero.

6. Space charge

Finally, we turn our focus to the role of space charge in nanoribbon bending. The local space charge density $\rho = \rho(z)$ is defined as the net charge associated with both free carriers³ and fixed ionic species⁴ integrated over a small volume element. Space charge is generated by the depletion or accumulation of free charge carriers, which produce the sheet charges σ_a and σ_b (on the Zn- and O-terminated surfaces, respectively) that are necessary to cancel surface polarity (Vanderbilt and King-Smith, 1993; Noguera, 2000; Harris et al., 2000; Allen et al., 2007). In order to maintain overall charge neutrality, the local space charge density must satisfy the balance $\sigma_a + \sigma_b + \int \rho dz = 0$. As before, the indices a and b correspond to values at the coordinates $z = H/2$ and $z = -H/2$, respectively.

One contribution to space charge is the movement of free carriers originating from defects (such as O vacancies or Zn interstitials) and/or dopants (donors or acceptors). When uniformly distributed, such carriers have a charge density qn_0 , where q is the charge of the carriers (for electrons, $q = -1.6 \times 10^{-19} \text{ C}$) and n_0 is the carrier concentration. When the carriers move to the surface of the crystal, they leave behind a depletion layer of ionized donors or acceptors with charge density ρ_0 , which in the case of complete depletion can be as great as $-qn_0$. Other sources of space charge are the inversion and accumulation layers that may form near nanoribbon faces (Harris et al., 2000; Allen et al., 2007; Sze, 1981).

Even without intentional doping, GaN and ZnO wafers typically contain free carriers with densities ranging from $n_0 = 10^{20}$ to 10^{25} m^{-3} (Harris et al., 2000; Allen et al., 2007). In the case of ZnO nanowires, the carrier density can reach as high as 10^{27} m^{-3} (Konenkamp et al., 2000). ZnO typically exhibits n-type semiconducting properties, although p-type ZnO has also been fabricated (Yuan et al., 2008; Braunstein et al., 2005). In subsequent calculations, we will assume, for the sake of convenience and because it is the most common case, that the nanoribbons are n-type (unless otherwise noted).

For an n-type nanoribbon, the free carriers will be negatively charged and are thus expected to accumulate on the Zn-terminated surface. Since the O-terminated surface has an effective negative charge due to O^{2-} surface ions, it will not attract negatively charged free carriers from the bulk and so $\sigma_b = 0$.⁵ Therefore, at $z = a$ there will be a sheet charge with a charge density $\sigma_a = -\int_b^a \rho(z) dz$. This carrier migration leaves a depletion layer of thickness H_d with $\rho(z) > 0$, whose properties govern nanoribbon bending through a piezoelectric coupling, to which we turn next.

6.1. Piezoelectric-induced deformation

The uniform stretch γ_0 and curvature κ are found by minimizing the total potential energy of the nanoribbon in Eq. (7). For pure bending, $\gamma_{11} = \gamma_0 - \kappa z$ and $\gamma_{33} = \gamma_{33}(z)$. At equilibrium Π must be stationary with respect to infinitesimal variations in the unknowns $\Phi(z)$, γ_0 , κ , and $\gamma_{33}(z)$. These conditions are equivalent to the boundary and differential forms of Gauss' Law in the Lagrangian (undeformed) description: $D_z(H/2) = -\sigma_a$, $D_z(-H/2) = \sigma_b$, and $\partial D_z / \partial z = \rho(z)$, the balance of stress and moment: $\int T_{xx} dz = \int T_{xx} z dz = 0$, and the condition for plane stress: $T_{zz} = 0$. In light of the constitutive equations, these balance laws imply

$$\gamma_0 = \frac{P_0}{\eta} - \frac{1}{H\eta} \int_{-H/2}^{H/2} \int_{-H/2}^z \rho(\tilde{z}) d\tilde{z} dz \quad \text{and} \quad \kappa = \frac{12}{H^3\eta} \int_{-H/2}^{H/2} z \int_{-H/2}^z \rho(\tilde{z}) d\tilde{z} dz, \quad (25)$$

where the constant η is expressed in (C.8) in terms of the piezoelectric coefficients; for ZnO, $\eta = 11.85 \text{ C/m}^2$. Eq. (25) establish the link between nanoribbon deformation and mobile charge density, and constitute a central result of this paper.

In order to both illustrate the physical implications of (25) and keep the calculations analytically tractable, we will only consider the simple cases where $\rho(z)$ is either spatially uniform ($H_d = H$; $\rho = \rho_0$) or restricted to a narrow region close to the (0001) surface ($H_d < H$; $\rho = \rho_0$ within the depletion layer and $\rho = 0$ elsewhere). In either case, it follows from (25) that

$$\gamma_0 = \frac{P_0}{\eta} - \frac{\rho_0 H_d^2}{2\eta H} \quad \text{and} \quad \kappa = \frac{\rho_0 H_d^2 (3H - 2H_d)}{\eta H^3}. \quad (26)$$

The above relationships express the stretch ($1 + \gamma_0$) and bending curvature (κ) as a function of the nanoribbon thickness (H), depth (H_d) and space charge (ρ_0) of the depletion layer, spontaneous polarization (P_0), and piezoelectric constants (η). In

³ Free carriers are point charges that can move through the lattice on experimental time scales. Examples include charged vacancies and interstitials or electrons and holes.

⁴ These do not move significantly on the time scale of experiments. Ionic species also include dopant species, like In^+ in ZnO.

⁵ The polarity at the $z = b$ face will induce strong band bending in the electronic structure of the crystal, resulting in the formation of an accumulation layer. In this case, σ_b will be equal and opposite to the charge in the accumulation layer. However, the thickness of the accumulation layer is small in comparison to H and so the accumulation layer can be treated as part of the $z = b$ face. In this case, the surface charge and charge in the accumulation layer cancel each other, leaving σ_b to be effectively equal to zero.

the remainder of this section, we focus on three idealized three depletion regimes defined by the length scales H , H_1 , and H_2 :

- (I) *Complete depletion* ($H < H_1$): All the free electrons accumulate on the Zn-terminated surface ($H_d = H$ and $\rho_0 = |q|n_0$).
- (II) *Uniform depletion* ($H_1 \leq H \leq H_2$): Some free electrons accumulate on the Zn-terminated surface while the rest are uniformly distributed throughout the interior ($H_d = H$ and $\rho_0 < |q|n_0$).
- (III) *Partial depletion* ($H > H_2$): Only free carriers near the surface are depleted ($H_d < H$).

The assumption that space charge is uniform within the depletion layer has been adopted for the sake of mathematical convenience and to allow for an algebraic expression of the predicted bending curvature. Experiments and more accurate theoretical models indicate that space charge is not uniformly distributed inside the depletion zone. Nonetheless, it is common practice in semiconductor physics to adopt the so-called “uniform depletion” model (Sze, 1981).

Complete depletion is expected to occur if the thickness of the nanoribbon is below a critical value $H_1 = P_0/|q|n_0$. In such a case, the surface charge $|\sigma_a| = |q|n_0H < P_0$ and is thus inadequate to balance surface polarity. Following from (26), $\gamma_0 = (P_0 + qn_0H/2)/\eta$ and $\kappa = -qn_0/\eta$, i.e., the bending radius $R = 1/\kappa$ is independent of H . However, if $H \geq H_1$ then surface polarity can be completely screened by the free carriers ($\sigma_a = -P_0$). For uniform depletion (i.e., $H_d = H$), this implies $\rho_0 = P_0/H$ and so it follows from (26) that $\gamma_0 = P_0/2\eta$ and $\kappa = P_0/\eta H$. In this case, the bending radius will be directly proportional to the nanoribbon thickness, i.e., $R = \eta H/P_0$.

If the depletion layer thickness H_d is too large then an inversion layer, which prevents further widening of the depleted region, will form. Specifically, H_d is bounded from the above by $H_d \leq H_2 = \min\{2\bar{\epsilon}E_g/P_0, \sqrt{2\bar{\epsilon}E_g/|q|n_0}\}$ (Harris et al., 2000; Allen et al., 2007), where E_g is the bandgap and

$$\bar{\epsilon} = \epsilon_{33} + \frac{g_{31}^2 C_{33} - 2g_{31}g_{33}C_{13} + g_{33}^2 C_{11}}{C_{11}C_{33} - C_{13}^2} \quad (27)$$

is the effective permittivity for a stress-free nanoribbon (i.e., $D_3 = P_0 + \bar{\epsilon}E_3$). In the case of ZnO, $E_g = 3.37$ V and $\bar{\epsilon} = 8.88 \times 10^{-11}$ F/m. For $10^{20} \leq n_0 \leq 10^{27} \text{ m}^{-3}$, H_1 is in the range 0.35 nm to 3.5 mm and H_2 ranges from 10.5 nm to 10 μm . Following from (26), partial depletion corresponds to a stronger dependence between bending radius and thickness: $R \approx \eta H^2/(3\rho_0 H_d^2)$. Upon increasing the nanoribbon thickness, we thus expect the bending radius to asymptotically exhibit a quadratic dependence on nanoribbon thickness, with the details of the spatially varying charge distribution only affecting the prefactor. In this sense, all such piezoelectric films should display universal behavior with regard to bending.

It is interesting to note that in all three regimes, κ vanishes for non-piezoelectric materials since $\eta = \infty$ when the piezoelectric coupling coefficients are zero. Since $\kappa > 0$, the ribbon bends towards the Zn-terminated face. If, however, the nanoribbon is p-type ($q < 0$), then the same analysis predicts a negative curvature (the ribbon bends towards the O-terminated surface). Theoretical predictions for the three depletion regimes are presented in Fig. 3(a) for $\eta = 11.85 \text{ C/m}^2$, $P_0 = 0.057 \text{ C/m}^2$, and varying values of carrier concentration n_0 and nanoribbon thickness H . For $n_0 = 10^{26} \text{ m}^{-3}$, the relationship between bending radius and thickness appears as in Fig. 3(b), with critical thicknesses calculated to be $H_1 = 3.6 \text{ nm}$ and $H_2 = 10.5 \text{ nm}$. Also shown in Fig. 3(b) are theoretical predictions for AlN and GaN.

In Figs. 4(a) and (b), we superimpose theoretical curves for ZnO on the experimental data (Hughes and Wang, 2004) to demonstrate the agreement between theory and experiment. The agreement is reasonable given that there are no

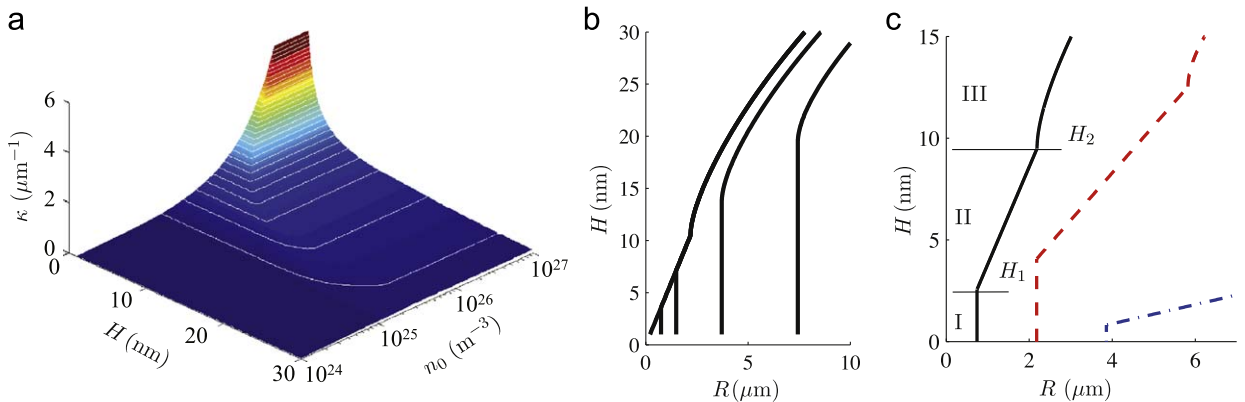


Fig. 3. (a) Predicted curvature (κ) as a function of nanoribbon thickness (H) and carrier concentration (n_0) for ZnO ($P_0 = 0.057 \text{ C/m}^2$ and $\eta = 11.85 \text{ C/m}^2$). (b) Bending radius ($R = 1/\kappa$) versus thickness; from right: $n_0 = 10^{25}, 2 \times 10^{25}, 5 \times 10^{25}, 10^{26}, 10^{27} \text{ m}^{-3}$. (c) Theoretical predictions with $n_0 = 10^{26} \text{ m}^{-3}$ for (solid black) ZnO, (dashed red) AlN, and (dash-dot blue) GaN. The three regimes are shown for the ZnO nanoribbon: (I) complete depletion, (II) uniform depletion, (III) partial depletion. (For interpretation of the references to color in this figure legend, the reader is referred to the web version of this article.)

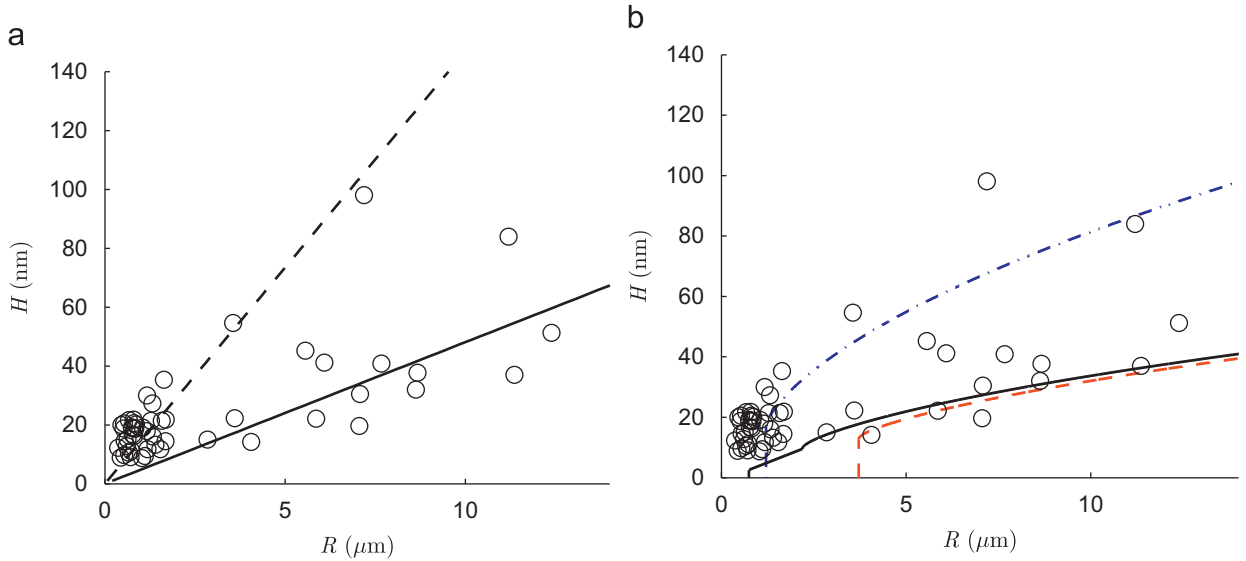


Fig. 4. (a) Experimentally measured values (open circles) (Hughes and Wang, 2004) and theoretical predictions for the bending radius of curvature (R) versus thickness (H) of ZnO nanoribbons. The solid and dotted lines represent the theoretical prediction of $R = \eta H / P_0$ for $\eta = 11.85$ and 3.88 C/m², respectively. (b) Theoretical predictions based on the three depletion regimes: (solid black) $n_0 = 10^{26}$ m⁻³ and $\eta = 11.85$ C/m², (dashed red) $n_0 = 2 \times 10^{25}$ and $\eta = 11.85$ C/m², (dash-dot blue) $n_0 = 2 \times 10^{25}$ and $\eta = 3.88$ C/m². (For interpretation of the references to color in this figure legend, the reader is referred to the web version of this article.)

adjustable parameters, although the theory appears to more accurately represent a lower bound on the thickness required to achieve the observed curvature. Theoretical and empirical agreement might be improved by including additional effects not addressed in the analysis, such as surface stress and crystal defects (Tu et al., 2006), that can increase the spontaneous curvature and cause the theoretical curves in Fig. 4(b) to shift to the left. Lastly, the average elastic modulus of ZnO nanowires has been measured to be 40 GPa (Manoharan et al., 2008), well below the bulk value of 210 GPa used to evaluate η . Reducing the stiffness coefficients by 80%, we find strong agreement with a carrier concentration of $n_0 = 2 \times 10^{25}$ m⁻³, as seen in Fig. 4. While still high, this is an order of magnitude less than the values measured for a ZnO nanowire (Konenkamp et al., 2000; Sero et al., 2006).

6.2. Depletion-induced electrostatic deflection

Space charge can induce ribbon bending even in the absence of piezoelectric coupling ($\mathbf{g} = 0$). In the case of a ZnO nanoribbon, the formation of a depletion layer near the Zn-terminated surface results in a non-uniform distribution of electrostatic stresses. These stresses arise from the electrostatic repulsion of free carriers and lattice charges and induce small but significant elastic strain. This mechanism of strain through electrostatic repulsion is distinct from electrostriction, which had been previously used to explain the bending of polymer films inside an electric field (Watanabe, 2007). In electrostriction, lattice distortion is induced by the asymmetric rearrangement of otherwise centrosymmetric ions under an electric field (Kay, 1955).

In the limit of uniform depletion ($H_d = H$, $\rho = P_0/H$), bending the nanoribbon with a constant curvature κ decreases the potential energy by approximately $wP_0^2H^2\kappa/24\epsilon_{33}$. For a non-piezoelectric crystal where only elasticity and electrostatics contribute to the bending energy, analysis predicts a bending curvature of approximately $\kappa^* = P_0^2/Y\epsilon_{33}H$. General expressions for the electrostatic energy in terms of H_d are presented in Appendix D.

A typical nanoribbon has width and thickness on the order of $w = 50$ nm, and $H = 10$ nm respectively. For $Y = C_{11} - C_{13}^2/C_{33} = 158$ GPa, $\epsilon_{33} = 7.38 \times 10^{-11}$ F/m (Ding and Chen, 2001), and $\sigma = P_0 = 0.057$ C/m², it follows that $R^* = 1/\kappa^* \approx 36$ μ m. This is two orders of magnitude greater than the smallest values that have been measured experimentally. Moreover, when bending with a radius of $R = 1$ μ m, the electrostatic energy decreases by approximately 10^{-11} J/m, which is a factor of 30 less than the corresponding elastic strain energy. While electrostatics within the depletion layer may have a role in nanoribbon bending, these results suggest that its contribution is small compared to that of piezoelectric coupling. Nonetheless, it is a mechanism that may govern the deformation of non-piezoelectric ribbons and films.

7. Discussion

Spontaneous bending has been observed for ZnO and several other wurtzite-structured nanoribbons with $\pm(0001)$ faces. Several models have been proposed to explain this bending. Because bending in such materials necessarily involves

many competing effects (including surface stress, elasticity, electrostatics, piezoelectricity, etc.), it has not been possible to identify the dominant physics based on analyses of individual effects or small groups of effects. To address this issue, we have performed a comprehensive thermodynamic analysis that simultaneously considers the contributions of elasticity, surface stress, surface charge, space charge, spontaneous polarization, and piezoelectricity.

Surface stress is rejected as the main cause for bending since it is too weak to account for the magnitude of the observed curvature and is not consistent with the observation that ZnO nanoribbons can bend towards either face. The piezoelectric response generated by surface charge only cause the nanoribbon to change length but do not induce curvature. If space charge is present, such as from the formation of a depletion layer, then electrostatics alone could lead to spontaneous bending. However, the radius of curvature predicted by the depletion-induced electrostatic deflection model is one to two orders of magnitude greater than the experimentally observed value. Hence, this mechanism would have at best a secondary contribution to the spontaneous nanoribbon bending.

Space charge induced piezoelectric interaction is the only mechanism that explains the following experimental observations: the magnitude and sign of the experimentally measured radii of curvature, how this curvature depends on film thickness, and the dependency of curvature on dopant concentration. The good agreement between theory and experiment is obtained with no adjustable parameters.

It is important to note that piezoelectric coupling is essential for space charge induced bending; elasticity or electrostatics alone are not sufficient. Referring to Eq. (C.8), the parameter η goes to ∞ when the coupling coefficients g_{ij} vanish. Though necessary, piezoelectricity alone is not sufficient—bending requires free charge carriers (that can move on time scales that are experimentally relevant) and polarized surfaces to deplete those carriers from the interior. In the absence of these properties, spontaneous bending is still possible but only under the much weaker surface stress anisotropy effect.

Although there is strong support for the piezoelectric model in Section 6.1, there are still several open issues that must be addressed. In particular, it would be useful to compare the magnitude and direction of bending with estimates of the carrier concentration and type (n-type or p-type). This would confirm the theoretical prediction that p-type ribbons bend towards the O-terminated face. There are also several areas in which the theoretical models can be improved. Broader and more accurate predictions might be obtained by expanding the definition of electric displacement to include higher order contributions such as electrostriction. Space charge distribution and characteristics of the anticipated depletion layer also deserve further investigation, especially with respect to alternative mechanisms for surface stability such as charge adsorption and surface reconstruction (Noguera, 2000).

8. Conclusion

The present analysis provides an appropriate framework to examine other non-planar nanoribbon geometries such as nanosprings and helices and to incorporate the energetic contributions of lattice defects and crystal domain interfaces. In addition to explaining the experimentally observed nanoribbon curvature, the thermodynamic analysis can be used to address mechanical and electromechanical properties of piezoelectric nanoribbons such as the effective Young's modulus (Manoharan et al., 2008; Wang and Li, 2006), resonance, and bending induced power generation (Wang and Song, 2006).

Acknowledgments

The authors are grateful to Zhang Yong Wei (National University of Singapore), Craig Arnold and Jason Fleischer (Princeton University) for useful discussions and to Will Hughes (Boise State) for providing experimental data from Hughes and Wang (2004). This work has been supported in part by an NSF-DMR Grant no. 0449184 (MH).

Appendix A. Derivation of governing thermodynamic equations

The variations (8) lead to the following variation in Π :

$$\delta\Pi = \int_B \left\{ \frac{\partial h}{\partial \nabla \mathbf{u}} : \nabla \delta \mathbf{u} + \frac{\partial h}{\partial \nabla \Phi} \cdot \nabla \delta \Phi + \rho \delta \Phi \right\} dV + \int_{\partial B} \{ \sigma \delta \Phi - \hat{\mathbf{t}} \cdot \delta \mathbf{u} \} dS. \quad (\text{A.1})$$

The above expression may be simplified first by noting that

$$\frac{\partial h}{\partial \nabla \mathbf{u}} = \frac{\partial h}{\partial \gamma} : \frac{\partial \gamma}{\partial \nabla \mathbf{u}} = \frac{1}{2} \mathbf{T} : \left(\frac{\partial \nabla \mathbf{u}}{\partial \nabla \mathbf{u}} + \frac{\partial \nabla \mathbf{u}^T}{\partial \nabla \mathbf{u}} \right) \Rightarrow \frac{\partial h}{\partial \nabla \mathbf{u}} = \frac{1}{2} (\mathbf{T} + \mathbf{T}^T) = \mathbf{T} \quad (\text{A.2})$$

and

$$\frac{\partial h}{\partial \nabla \Phi} = -\frac{\partial h}{\partial \mathbf{E}} = \mathbf{D}. \quad (\text{A.3})$$

(In (A.2), the derivation is only valid for an infinitesimal strain measure (1). Nonetheless, $\partial h / \partial \nabla \mathbf{u} = \mathbf{T}$ is generally true for all elastic strain measures provided that \mathbf{T} is defined as the first Piola–Kirchoff stress tensor.) Next, by the chain rule (Bertram, 2005),

$$\nabla \cdot (\mathbf{T} \cdot \delta \mathbf{u}) = (\nabla \cdot \mathbf{T}) \cdot \delta \mathbf{u} + \mathbf{T} : \nabla \delta \mathbf{u} \quad \text{and} \quad \nabla \cdot (\mathbf{D} \cdot \delta \Phi) = (\nabla \cdot \mathbf{D}) \delta \Phi + \mathbf{D} \cdot \nabla \delta \Phi. \quad (\text{A.4})$$

Moreover, by the divergence theorem (and again noting that $\mathbf{T} = \mathbf{T}^T$)

$$\int_B \nabla \cdot (\mathbf{T} \cdot \delta \mathbf{u}) dV = \int_{\partial B} (\mathbf{T} \cdot \mathbf{n}) \cdot \delta \mathbf{u} dS \quad \text{and} \quad \int_B \nabla \cdot (\mathbf{D} \delta \Phi) dV = \int_{\partial B} (\mathbf{D} \cdot \mathbf{n}) \delta \Phi dS, \quad (\text{A.5})$$

where \mathbf{n} is the unit normal to B . Hence,

$$\delta \Pi = \int_B \{-\nabla \cdot \mathbf{T}\} \cdot \delta \mathbf{u} dV + \int_{\partial B} \{\mathbf{T} \cdot \mathbf{n} - \hat{\mathbf{t}}\} \cdot \delta \mathbf{u} dS + \int_B \{-\nabla \cdot \mathbf{D} + \rho\} \delta \Phi dV + \int_{\partial B} \{\sigma + \mathbf{D} \cdot \mathbf{n}\} \delta \Phi dS. \quad (\text{A.6})$$

Since $\delta \mathbf{u}$ and $\delta \Phi$ are arbitrary, the variation $\delta \Pi$ vanishes if and only if the balance equations (9) and (10) are satisfied.

Appendix B. Solution for surface stress

Ignoring spontaneous polarization, surface charge, and space charge (i.e., $\mathbf{P}_0 = \sigma = \rho = 0$) it follows that $\mathbf{D} = 0$. From the constitutive relations (18) and (19), this implies $E_1 = 0$ and $E_3 = -(\mathbf{g}_{31}/\epsilon_{33})\gamma_{11} - (\mathbf{g}_{33}/\epsilon_{33})\gamma_{33}$. In the absence of surface traction, i.e., $\hat{\mathbf{t}} = 0$, the total potential energy of the system reduces to

$$\Pi = \left\{ -f_a(\gamma_0 - \kappa a) - f_b(\gamma_0 - \kappa b) + \int_b^a h dz \right\} wL, \quad (\text{B.1})$$

where the enthalpy density is

$$h = \frac{1}{2} \left(C_{11} + \frac{\mathbf{g}_{31}^2}{\epsilon_{33}} \right) (\gamma_0 - \kappa z)^2 + \left(C_{11} + \frac{\mathbf{g}_{31}\mathbf{g}_{33}}{\epsilon_{33}} \right) (\gamma_0 - \kappa z) \gamma_{33} + \frac{1}{2} \left(C_{11} + \frac{\mathbf{g}_{33}^2}{\epsilon_{33}} \right) \gamma_{33}^2. \quad (\text{B.2})$$

At equilibrium, Π must be minimized with respect to γ_0 , κ , and $\gamma_{33} = \gamma_{33}(z)$. First consider the minimization of Π with respect to γ_{33} , which implies $\partial h / \partial \gamma_{33} = 0$. Solving $\partial h / \partial \gamma_{33} = 0$ for γ_{33} and substituting this expression for γ_{33} into h yields $h = (1/2)\bar{C}(\gamma_0 - \kappa z)^2$, where

$$\bar{C} = C_{11} - \frac{C_{13}^2 \epsilon_{33} + 2C_{13}\mathbf{g}_{31}\mathbf{g}_{33} - C_{33}\mathbf{g}_{31}^2}{\epsilon_{33}C_{33} + \mathbf{g}_{33}^2}. \quad (\text{B.3})$$

For ZnO, $\bar{C} = 175$ GPa. Substituting h into Π and integrating yields an algebraic expression for the potential energy. Lastly, solving $\partial \Pi / \partial \gamma_0 = 0$ and $\partial \Pi / \partial \kappa = 0$ for γ_0 and κ yields

$$\gamma_0 = \frac{f_a + f_b}{CH} \quad \text{and} \quad \kappa = \frac{6(f_b - f_a)}{CH^2}. \quad (\text{B.4})$$

Appendix C. Derivation of nanoribbon stretch and curvature

Because of the spatial variation in ρ , the restriction (13) on the kinematics is no longer valid and should be regarded as a first order approximation of a more complex deformation field. Governing equations are rederived by minimizing the total potential energy Π with respect to the free variables γ_0 , κ , $\gamma_{33} = \gamma_{33}(z)$, and $\Phi = \Phi(z)$.

In addition to the kinematic restriction (13), we also apply the restriction $E_1 = 0$, which follows from (17) and the assumption that $T_{13} = 0$. Hence,

$$\Pi = \left\{ \sigma_a \Phi(a) + \sigma_b \Phi(b) + \int_{z^*}^a \mathcal{L} dz + \int_b^{z^*} \mathcal{L} dz \right\} wL, \quad (\text{C.1})$$

where $z^* = H/2 - H_d$. The Lagrangian, \mathcal{L} , is

$$\mathcal{L} = \frac{1}{2} C_{11} \gamma_{11}^2 + C_{13} \gamma_{11} \gamma_{33} + \frac{1}{2} C_{33} \gamma_{33}^2 + \mathbf{g}_{31} \Phi' \gamma_{11} + \mathbf{g}_{33} \Phi' \gamma_{33} - \frac{1}{2} \epsilon_{33} \Phi'^2 + P_0 \Phi' + \rho \Phi, \quad (\text{C.2})$$

where the prime denotes the derivative with respect to the coordinate z . The conditions for equilibrium thus become

$$\frac{\partial \Pi}{\partial \gamma_0} = 0, \quad \frac{\partial \Pi}{\partial \kappa} = 0, \quad \frac{\partial \mathcal{L}}{\partial \gamma_{33}} = 0, \quad \delta_\Phi \Pi = 0. \quad (\text{C.3})$$

The first two conditions in (C.3) imply the balance of stress and moment when integrated over the cross-section: $\int T_{11} dz = \int T_{11} z dz = 0$. Following the Euler–Lagrange equation, the third condition implies plane stress: $T_{33} = 0$. In order to

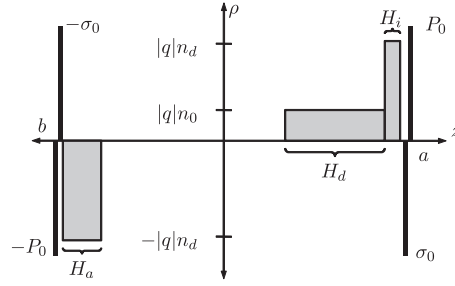


Fig. C.1. Charge distribution for an n-type nanoribbon ($q = -1.6 \times 10^{-19}$ C). The black regions at $z = a$ and $z = b$ represent surface charge. Near the $z = a$ surface is an inversion and depletion layer of thickness H_i and H_d , respectively. On the opposite side, near $z = b$ is an accumulation layer of thickness H_a . For large carrier concentrations ($n_0 \sim 10^{25} - 10^{27}$ m $^{-3}$), an inversion layer is not expected to form (Sze, 1981).

evaluate the fourth condition in (C.3) we consider electrostatically admissible variations of the form

$$\Phi \rightarrow \Phi + \delta\Phi \quad \text{and} \quad \Phi' \rightarrow \Phi' + \delta\Phi'. \quad (\text{C.4})$$

It is assumed that Φ and Φ' are not prescribed anywhere in or on the nanoribbon. This implies that the variations $\delta\Phi$ and $\delta\Phi'$ are arbitrary (though infinitesimally small) $\forall z \in [b, a]$.⁶ The corresponding variation of Π is evaluated using the calculus of variations and Leibniz's integration rule and vanishes when the boundary conditions and differential form of Gauss's law are satisfied in the Lagrangian (undeformed) description:

$$D_3(a) = -\sigma_a, \quad D_3(b) = \sigma_b, \quad D_3(z_+^*) = D_3(z_-^*), \quad \frac{dD_3}{dz} = \rho, \quad (\text{C.5})$$

where $\chi(z_{\pm}^*) = \lim_{\tau \rightarrow 0} \chi(z^* \pm \tau)$.

Simultaneously solving the constitutive equations (16) and (19) along with the condition $T_{33} = 0$ yield algebraic expressions for γ_{33} and E_3 in terms of D_3 and γ_{11} . Next, these expressions are substituted into (15) in order to calculate T_{11} in terms of γ_{11} and D_3 . For $\gamma_{11} = \gamma_0 - \kappa z$, it follows from the balance laws $\int T_{11} dz = 0$ and $\int T_{11} z dz = 0$ that

$$\gamma_0 = \frac{P_0}{\eta} - \frac{1}{H\eta} \int_a D_3 dz \quad \text{and} \quad \kappa = \frac{12}{H^3\eta} \int_a D_3 z dz, \quad (\text{C.6})$$

where

$$D_3(z) = \int_a^z \rho(\tilde{z}) d\tilde{z} \quad (\text{C.7})$$

and

$$\eta = \frac{-2g_{31}C_{13}g_{33} + C_{33}g_{31}^2 + C_{11}g_{33}^2 - \varepsilon_{33}C_{13}^2 + \varepsilon_{33}C_{33}C_{11}}{C_{13}g_{33} - C_{33}g_{31}}. \quad (\text{C.8})$$

For ZnO, $\eta = 11.85$ C/m 2 .

If the ribbon has a thickness $H > H_2$, then it is reasonable to assume that depletion will be limited to a surface layer of thickness $H_d \sim H_2$. Hence, the space charge density $\rho = \rho(z)$ will be piecewise constant: $\rho = \rho_0$ for $z \in (a - H_d, a)$, $\rho = 0$ for $z \in (b, a - H_d)$, $\sigma(a) = \rho_0 H_d$, and $\sigma(b) = 0$. The schematic in Fig. C.1 represents a piecewise constant approximation of the space charge distribution $\rho = \rho(z)$ for an n-type semiconductor (Sze, 1981). Here, H_d , H_i , and H_a denote the thickness of the depletion, inversion, and accumulation layers, respectively. The strong band bending induced by spontaneous polarization results in degenerate carrier densities in the inversion and accumulation layers with concentrations on the order of (Harris et al., 2000)

$$n_d = \frac{1}{3\pi^2} \left(\frac{2mq\Phi_s}{\hbar^2} \right)^{3/2}. \quad (\text{C.9})$$

Here, $m = \mu m_e$ is the electron effective mass, $m_e = 9.109 \times 10^{-34}$ kg is the electron mass, Φ_s is the surface potential, and $\hbar = 1.054 \times 10^{-34}$ J/s is the reduced Planck's constant. Using an approximate analytical method, Harris et al. (2000) estimate that for GaN ($P_0 = 0.029$ C/m 2 , $\varepsilon_{33} = 8.41 \times 10^{-11}$ F/m, and $\mu = 0.22$) $\Phi_s = 0.47$ V. Applying the same method to ZnO ($P_0 = 0.057$ C/m 2 , $\varepsilon_{33} = 7.38 \times 10^{-11}$ F/m, and $\mu = 0.19$), we calculate $\Phi_s = 0.91$ V. Substituting this value into (C.9), the electron and hole concentrations in the accumulation and inversion layers, respectively, are estimated to be on the order of $n_d = 3.8 \times 10^{26}$ m $^{-3}$.

⁶ If, for example, a potential Φ_a were prescribed at $z = a = H/2$, then $\delta\Phi_a = 0$ would be the only electrostatically admissible variation at that point. Physically, this would require the presence of an electrode and power supply that could compensate for the additional energy needed to maintain the prescribed potential. Such a condition will not be considered in the remaining analysis.

Appendix D. Depletion-induced electrostatic deflection

As in the capacitor model of Section 5.1, $Q = 2\pi wR\sigma$ represents the effective surface charge associated with surface polarity and $\sigma = P_0$ is the effective sheet charge density on the Zn-terminated surface ($z = H/2$). For a depletion layer of thickness H_d , the surface polarity is fully neutralized with a space charge density $\rho_0 = \sigma/H_d$.

When planar and in the absence of piezoelectric coupling, charge depletion results in an internal electric field $E_3(z) = \sigma/\epsilon_{33}$ for $z \in [-H/2, H/2 - H_d]$ and $E_3(z) = \sigma(z - H/2)/\epsilon_{33}H_d$ for $z \in [H/2 - H_d, H/2]$. The electrostatic energy per unit length along the nanoribbon is

$$\phi_1 = \int_{-H/2}^{H/2} \frac{1}{2} \epsilon_{33} E_3(z)^2 w dz = \frac{\sigma^2 w}{2\epsilon_{33}} (H - H_d) + \int_{H/2 - H_d}^{H/2} \frac{1}{2} \epsilon_{33} E_3(z)^2 w dz. \quad (D.1)$$

When forming a ring of radius R , the internal electric field becomes $E_3(r) = \sigma R(R - H/2 - r)/\epsilon_{33}H_d r$ for $r \in [R - H/2, R - H/2 + H_d]$ in the depletion layer, and $E_3(r) = \sigma R/\epsilon_{33}r$ for $r \in [R - H/2 + H_d, R + H/2]$. Here, $r \in [R - H/2, R + H/2]$ is the radial coordinate originating from the center of the nanoring. In this case, the electrostatic energy per unit length is

$$\phi_2 = \int_{R - H/2}^{R + H/2} \frac{1}{2} \epsilon_{33} E_3(r)^2 w dr = \int_{R - H/2}^{R - H/2 + H_d} \frac{1}{2} \epsilon_{33} E_3(r)^2 w dr + \frac{\sigma^2 R w}{2\epsilon_{33}} \ln\left(\frac{R + H/2}{R - H/2 + H_d}\right). \quad (D.2)$$

Noting that $H/R \ll 1$, it follows that to order $\mathcal{O}(H/R)^2$, the change in electrostatic energy per unit length is approximately

$$\Delta\phi = \phi_2 - \phi_1 \approx \frac{\sigma^2 w R}{2\epsilon_{33}} \left\{ -\frac{H_d}{3H} + \frac{1}{4} \left(\frac{H_d}{H}\right)^2 \right\} \left(\frac{H}{R}\right)^2. \quad (D.3)$$

References

- Allen, M.W., Miller, P., Reeves, R.J., Durbin, S.M., 2007. Influence of spontaneous polarization on the electrical and optical properties of bulk, single crystal ZnO. *Appl. Phys. Lett.* 90, 062104.
- Bernardini, F., Fiorentini, V., Vanderbilt, D., 1997. Spontaneous polarization and piezoelectric constants of III–V nitrides. *Phys. Rev. B* 56, R10024.
- Bertram, A., 2005. *Elasticity and Plasticity of Large Deformations*. Springer, Berlin.
- Braunstein, G., Muraviev, A., Saxena, H., Dhare, N., Richter, V., Kalish, R., 2005. p-Type doping of zinc oxide by arsenic ion implantation. *Appl. Phys. Lett.* 87, 192103.
- Cahn, J.W., Hanneman, R.E., 1964. (111) surface tensions of III–V compounds and their relationship to spontaneous bending of thin crystals. *Surf. Sci.* 1, 387–398.
- Ding, H.J., Chen, W.Q., 2001. *Three Dimensional Problems of Piezoelectricity*. Nova Science, Huntington, New York.
- Duan, J., Yang, S., Liu, H., Gong, J., Huang, H., Zhao, X., Tang, J., Zhang, R., Du, Y., 2005. AlN nanorings. *J. Cryst. Growth* 283, 291–296.
- Harris, J.J., Lee, K.J., Webb, J.B., Tang, H., Harrison, I., Flannery, L.B., Cheng, T.S., Foxon, C.T., 2000. The implications of spontaneous polarization effects for carrier transport measurements in GaN. *Semicond. Sci. Technol.* 15, 413–417.
- Huber, J.E., Fleck, N.A., Landis, C.M., McMeeking, R.M., 1999. A constitutive model for ferroelectric polycrystals. *J. Mech. Phys. Solids* 47, 1663–1697.
- Hughes, W.L., Wang, Z.L., 2004. Formation of piezoelectric single-crystal nanorings and nanobows. *J. Am. Chem. Soc.* 126, 6703–6709.
- Jian, J.K., Zhang, Z.H., Sun, Y.P., Lei, M., Chen, X.L., Wang, T.M., Wang, C., 2007. GaN nanorings: another example of spontaneous polarization-induced nanostructure. *J. Crystal Growth* 303, 427–432.
- Jogai, B., Albrecht, J.D., Pan, E., 2004. Energy levels in polarization superlattices a comparison of continuum strain models. *Semiconductor Sci. Technol.* 19, 733–741.
- Kay, H.F., 1955. Electrostriction. *Rep. Prog. Phys.* 18, 230–250.
- Konenkamp, R., Boedecker, K., Lux-Steiner, M.C., Poschenrieder, M., Zenia, F., Levy-Clement, C., Wagner, S., 2000. Thin film semiconductor deposition on free-standing ZnO columns. *Appl. Phys. Lett.* 77, 2575–2577.
- Kong, X.Y., Wang, Z.L., 2003. Spontaneous polarization-induced nanohelices, nanosprings, and nanorings of Piezoelectric nanobelts. *Nano Lett.* 3, 1625–1631.
- Kong, X.Y., Ding, Y., Yang, R., Wang, Z.L., 2004. Single crystal nanorings formed by epitaxial self-coiling of polar nanobelts. *Science* 303, 1348–1351.
- Kong, X.Y., Wang, Z.L., 2004. Polar-surface dominated ZnO nanobelts and the electrostatic energy induced nanohelices, nanosprings, and nanospirals. *Appl. Phys. Lett.* 84, 975–977.
- Manoharan, M.P., Desai, A.V., Neely, G., Haque, M.A., 2008. Synthesis and elastic characterization of zinc oxide nanowires. *J. Nanomaterials* 2008, 849745.
- Noguera, C., 2000. Polar oxide surfaces. *J. Phys. Condens. Matter* 12, R367–R410.
- Pak, Y.E., 1992. Linear electro-elastic fracture mechanics of piezoelectric materials. *Int. J. Fract.* 54, 79–100.
- Sero, I.M., Santiago, F.F., Denier, B., Bisquert, J., Zaera, R.T., Elias, J., Clement, C.L., 2006. Determination of carrier density of ZnO nanowires by electrochemical techniques. *Appl. Phys. Lett.* 89, 203117.
- Sze, S.M., 1981. *Physics of Semiconductor Devices*. Wiley, New York.
- Tu, Z.C., Li, Q.X., Hu, X., 2006. Theoretical determination of the necessary conditions for the formation of ZnO nanorings and nanohelices. *Phys. Rev. B* 73, 115402.
- Vanderbilt, D., King-Smith, R.D., 1993. Electric polarization as a bulk quantity and its relation to surface charge. *Phys. Rev. B* 43, 4442–4455.
- Wang, G., Li, X., 2006. Size dependency of the elastic modulus of ZnO nanowires: surface stress effect. *Appl. Phys. Lett.* 91, 231912.
- Wang, Z.L., 2004. Zinc oxide nanostructures: growth, properties and applications. *J. Phys. Condens. Matter* 16, R829–R858.
- Wang, Z.L., Song, J., 2006. Piezoelectric nanogenerators based on zinc oxide nanowire arrays. *Science* 312, 242–245.
- Watanabe, M., 2007. Model for the mechanism of the bending electrostriction in a polyurethane film. *J. Appl. Phys.* 46, 3495–3500.
- Yuan, G.D., Zhang, W.J., Jie, J.S., Fan, X., Zapfen, J.A., Leung, Y.H., Luo, L.B., Wang, P.F., Lee, C.S., Lee, S.T., 2008. p-Type ZnO nanowire arrays. *Nano Lett.* 8, 2591–2597.